Measurements of helicon wave propagation and Ar II emission

J. Scharer
University of Wisconsin, Madison, Wisconsin 53706

A. Degeling
Ecole Polytechnique Fédérale de Lausanne, Switzerland 1015

G. Borg and R. Boswell
Australian National University, Canberra, Australia 0200

(Received 29 November 2001; accepted 26 June 2002)

Wave magnetic field, optical and Langmuir probe measurements are carried out to examine fast and thermal electron contributions to plasma ionization in a helicon plasma source. For the optical measurements, an Ar II line (443 nm) with a particularly short lifetime (7 ns) is chosen to resolve the excitation rate within a radio frequency period (73.7 ns). Information is then obtained regarding the acceleration processes and their action on the electron distribution that caused the excitation. Spatio-temporal measurements of 443 nm peak emission show that the emission is modulated at the source frequency. The peak count phase of the modulation propagates along the plasma at a comparable speed as the local helicon wave phase velocity. Computer modeling utilizing lab data is carried out to examine wave field effects on electron acceleration and ionization contributions arising from non-Maxwellian fast electrons. © *2002 American Institute of Physics.*
[DOI: 10.1063/1.1501475]

I. INTRODUCTION

Helicon plasma sources produce moderate- to high-density plasmas at high efficiency. Their basic configuration is cylindrical, with an axial magnetic field, and one of various types of radio frequency (rf) antennas operating at a frequency between the ion and electron cyclotron frequencies. The rf energy ionizes the neutral target gas. The creation of plasma allows the antenna to excite a helicon wave, which, it is believed, enhances ionization through a variety of potential mechanisms. Helicon sources operate over a wide range of densities from $10^{10}-10^{13}/\mathrm{cm}^3$ and magnetic fields in the 20–1400 G range can result from a variety of physical processes. The physical processes that allow extremely efficient operation[1,2] in different operating regimes have been under extensive investigation in recent years. Collisional processes,[1,2] Landau damping,[2,3] antenna localized acceleration,[4,5] mode conversion near the lower hybrid frequency[6] and nonlinear trapping[7–10] of fast electrons have been examined for different operating regimes. The effects of an axial variation in the source static magnetic field and electron temperature anisotropy has been measured and modeled by Guo *et al.*[11] These efficient sources are considered for argon lasers,[12] silicon wafer etching,[13] materials processing, optical integrated circuit thin film creation,[14] space plasma simulation[15] and plasma thrusters for space vehicles.[16]

The central question in the physics of helicon sources is the cause of their highly efficient ionization and strong wave damping, which is not well explained by either collisional or Landau damping processes. A particular matter at issue is the existence, in some operating regimes, of a population of fast electrons comprising a non-Maxwellian component of the electron distribution, and the significance of its role in helicon ionization processes. Molvik *et al.*[10] reported evidence of such non-Maxwellian electrons using a gridded electron energy analyzer in a 15 cm diameter Nagoya Type-III helicon plasma source at power levels of 1.3 to 3.3 kW in 90–30 G fields. On the other hand, Maxwellian distributions over 2.5 orders of magnitude of the electron energy distribution were observed in a 10 cm diameter Nagoya Type-III helicon plasma source by Blackwell and Chen[17] at 1 kW power levels at 360 G. It should be noted that these experiments were carried out under substantially different plasma conditions, illustrating that helicon source ionization mechanisms can be sensitively dependent on the plasma density, magnetic field, and wave power. Moreover, the use of gridded energy analyzers and Langmuir probes must be carefully checked. Their introduction can allow sheaths and potential variations on grids to occur which can influence electron distribution function measurements in rf heating experiments. Ellingboe *et al.*[9] in a research letter reported measurements of Ar II emission at 443 nm and 2 kW coupled powers for a double-saddle type antenna. The emission was found to be modulated at the rf and peaks in emission were found to propagate along the source in phase with the measured helicon wave magnetic field.

In this paper we report on experiments performed on the WOMBAT[7] helicon experimental facility in which were created argon plasmas with densities in the range $10^{11}-10^{12}/\mathrm{cm}^3$. This work extends the results of Ellingboe *et al.* by carrying out measurements of density, wave B_z field and optical emission for a helicon source energized by a double-half-turn antenna. The optical measurements are of the Ar II line at 443 nm. The ionic state, Ar^+, has a threshold 15.6 eV above the neutral ground state, an excited metastable ionic state, $Ar^{+}*$, has a threshold 30 eV above the ground state and the 443 nm emission upper state is 35 eV above the

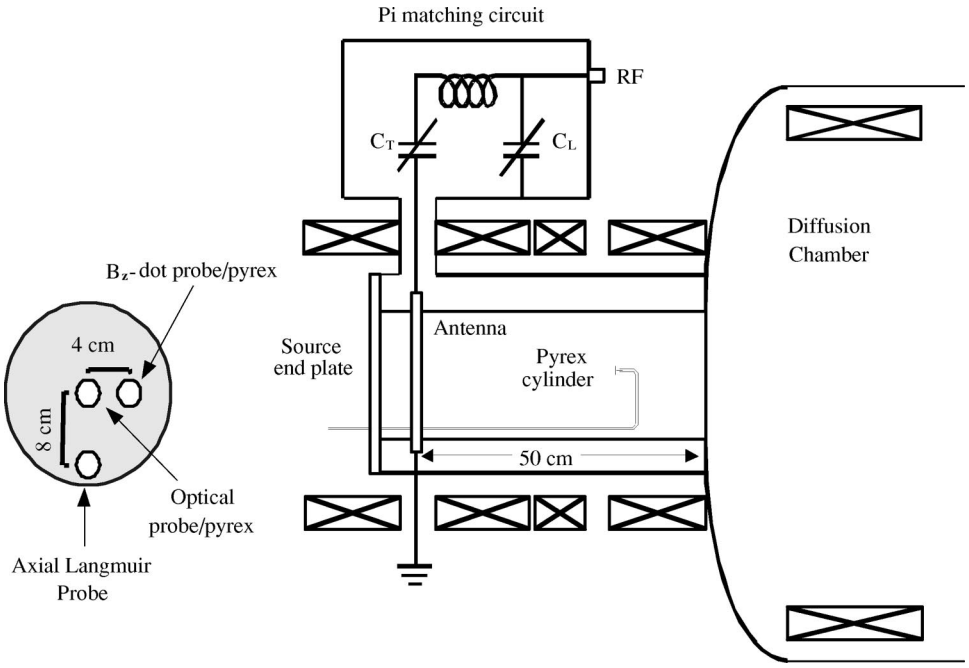

FIG. 1. WOMBAT experiment and diagnostic probes.

ground state.[18] The upper Ar II 443 nm emission state can be excited directly from the atomic ground state or from the ionic state by electron collisions. Thus, electrons of fairly high energy are required to directly populate these states, and emission at 443 nm is indicative of their presence.

Our objective in this paper is to show that substantial non-Maxwellian contributions to the source ionization for this regime can exist when excited by a double-half-turn antenna. Experimental measurements of the wave B_z magnetic field components are compared with those predicted by the ANTENAII[19] full wave boundary code for helicon modeling. The code also determines the wave electric fields consistent with the helicon wave hot plasma dielectric tensor. The role of the Trivelpiece–Gould mode in the core plasma is negligible for these parameters. The corresponding wave E_z field produced by the code is incorporated in a nonlinear[5] one-dimensional kinetic numerical model that illustrates the evolution of a non-Maxwellian electron distribution and enhanced argon ionization above what a Maxwellian distribution would produce under these experimental conditions.

The rest of the paper is organized as follows. In Sec. II we discuss the experimental apparatus. In Sec. III we discuss the experimental measurements which include wave power coupled and tuning to obtain a time-independent density characteristic, plasma density profiles, axial wave magnetic field amplitude and phase and wave-correlated Ar II 443 emission. These measurements allow one to correlate the wave characteristics with Ar II emission which is indicative of fast electron effects. In Sec. IV we carry out a modeling of the antenna, plasma and experimental boundary characteristics to obtain wave fields comparable to that observed experimentally. These are used in a wave acceleration code to predict the resulting electron distribution and enhanced ionization, which differ from that resulting from a Maxwellian distribution. In Sec. V we summarize the results and conclude that non-Maxwellian electron distributions are present for these moderate density helicon plasma source conditions.

II. EXPERIMENTAL APPARATUS

The experiments were carried out on the WOMBAT[7] experimental facility which consists of a 20 cm diameter, 50 cm long Pyrex source tube connected on axis to a 90 cm diameter, 2.5 m long stainless tube diffusion chamber. The other end of the source tube is terminated by a stainless steel end plate through which movable Langmuir, B-dot, and optical probes were inserted at different radii as noted in Fig. 1. External solenoids surrounding the source and an internal solenoid in the diffusion chamber provide a low dc magnetic field of 100 G in the source, decreasing monotonically to 60 G in the diffusion chamber. A base pressure of 6×10^{-6} Torr is maintained by a 300 L/s turbo molecular pump, and an argon pressure of 3 mTorr is set using a mass flow controller during experiments. Rf power at 2.3 kW at 13.56 MHz is coupled to the plasma via a matching network connected to a 1 cm wide, 20 cm diameter, double-half-turn copper coil located 7.5 cm from the conducting end plate. Measurements using the Langmuir, B-dot and optical probes inserted at different radii as shown in Fig. 1 were taken during a series of 50 repeated 4 ms plasma pulses, each containing a 1 ms window where plasm density a conditions were stationary and repeatable. Axial profiles of the density, wave magnetic field amplitude and phase and optical emission counts and phase relative to the rf period during this 1 ms window were obtained by incrementing the probe position after the plasma pulses.

The Langmuir probe used in this experiment consists of a tungsten wire with an exposed area of 0.5 cm^2 and 1 cm length which is surrounded by a ceramic tube which is in turn inserted into a grounded stainless steel shaft with a right

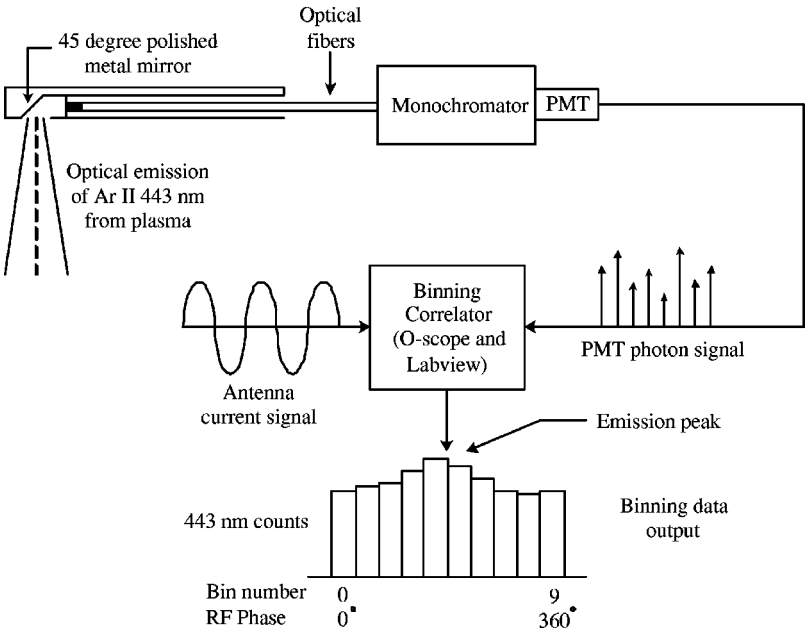

FIG. 2. Optical probe and rf correlation diagnostic.

angle bend. The axial length is about 60 cm, and it passes through the end plate port at a radius of 8 cm, allowing axial and radial scans to be made throughout the source region. This probe is used in the ion saturation region (-70 Volts) which is used to estimate the plasma density, n_e, according to the expression $I_{\mathrm{sat}}=0.6\,A\,n_e e v_{\mathrm{B}}$, where A is the probe area, e is the electronic charge and v_{B} is the Bohm velocity. Previous measurements in WOMBAT have been made with this source which indicate an electron temperature of 3 eV, yielding a Bohm velocity of 2.8×10^3 m/s in argon. Axial density measurements were made with the tip at $r=5$ cm. During optical scans the probe was left at a position $z=20$ cm and the tip was moved to an outer radius near the edge ($r=8$ cm) to ensure the probe did not affect optical measurements. Radial scans of density showed a broad, centrally peaked density profile, with the density decreasing substantially for radii greater than 5 cm.

The wave B_z field loop probe was mounted on a dielectric rod at a radius of 4 cm and was introduced through a re-entrant Pyrex tube of diameter 1.5 cm. It was removed for all optical emission and density scans. The optical probe was inserted through a re-entrant Pyrex tube of diameter 1.5 cm at a 4 cm radius and moved from $z=7.5$ cm to $z=60$ cm.

The B-dot probe that measured the axial component of the radiofrequency magnetic field, B_z, was made by wrapping ten turns of fine insulated copper wire on one end of a hollow dielectric tube of 1 cm diameter. The copper wires were run along the inside of the tube as a twisted pair. The rod was inserted into a Pyrex re-entrant glass tube at a radius of 4 cm from the axis through the end plate such that the plane of the probe coil was perpendicular to the z-direction. The rf signal on the twisted pair consists of a differential signal produced by magnetic induction across the probe coil and a common mode signal caused by electrostatic pickup along the probe wires. These signals are separated with a rejection ratio of 50:1 using a hybrid combiner circuit. The magnetic field amplitude and phase at the location of the B-dot probe were obtained by inputting the differential signal from the hybrid combiner to a 500 MHz digital oscilloscope with the reference phase input taken from the rf generator using a directional coupler. We took two scope traces of the wave B_z field at each position, separated by 10 seconds with a shot-to-shot repeatability within 5%. The rod was moved along the axis to obtain wave B_z amplitude and phase data as a function of the z position. The data were stored by means of a Labview Virtual Instrument (VI) program, and an IDL program was used to evaluate it and produce axial B_z variation graphics as a function of time. The magnetic probe was removed during all Langmuir probe and optical probe measurements.

Optical emission from the plasma was measured within a 7 ns time resolution by means of an axially centered optical probe that viewed the source emission across the radius as a function of axial position. The probe consisted of a 0.8 m long, 1 cm diameter tube at the end of which was attached a small, flat, polished stainless steel surface angled at 45 degrees to reflect the plasma emission into an optical fiber bundle located inside the tube. It was inserted into a clean re-entrant glass tube mounted on the center of the end plate. The 1 cm optical probe consisted of a 45 degree polished reflector section on stainless steel which was fed to an array of fibers located 3 cm from it. An overall view of the optical probe diagnostic including the phase correlation with the radiofrequency signal is shown in Fig. 2. Optical measurements of the probe using a laser source showed that it has a narrow acceptance angle of ±5 degrees from the perpendicular direction so that the probe has excellent axial resolution. The two-meter fiber array feeds the optical signal to a linear array which is input to a 200 micron entrance and exit slit of a Spex 0.5 m monochromator. The output of the monochromator was tuned to the 443.06 nm Ar II emission line which was measured by a photomultiplier. This line was chosen because it is isolated from other Ar emission lines, has an upper state with a threshold 20 eV above the argon

ionic state and 35 eV above the neutral argon state so that its emission is representative of fast electron effects in a helicon plasma source. It also has a short lifetime of 6.72 ns[18] so it can be correlated with the instantaneous phase of the 13.56 MHz rf signal. The lifetime of the Ar II state allows for a ± 10 percent variation in the emission peak relative to the wave period. In addition, there is a 5 ns uncertainty in the photomultiplier transit time that causes a $\pm 7\%$ uncertainty relative to the rf wave period and phase velocity. It should also be noted that a substantial additional deviation between the local wave phase velocity and emission peak can occur due to a broad distribution of Ar II upper state excitation electrons that can be created about the local wave phase velocity.

The 443 nm emission signal detected by the probe was sent to a dual channel 500 MHz Textronix digital oscilloscope capable of storing 2×10^5 samples during a trace. We took 50 shots, separated by 10 seconds, of 1 ms duration where the density was constant, after the 1 ms initial transient with the 1 Gs/s scope to obtain emission data at each position. A rf phase reference signal was provided to the oscilloscope by a directional coupler coupled to the rf generator. A photon counting virtual instrument (VI) was developed using Labview software to correlate the time of the 443 nm emission with the rf phase. The phase at which each photon entered the photomultiplier was obtained from these two signals on the oscilloscope using a threshold detection scheme. A binning algorithm with linear interpolation between bin centers was used to create a histogram of the photon counts as a function of phase. A total of ten bins for the 443 nm emission were used, which corresponds to a time resolution rf phase resolution of about 7 ns, or 36 degrees of an rf cycle. This system was carefully checked by correctly reproducing the modulation index of a laser signal modulated at 10 MHz. The optical probe was also blanked and the rf plasma system operated at 2.6 kW of power to ensure that there was a low level of photomultiplier noise and that there was no extraneous path for pickup from the system affecting the measurement. Random photon bin counting yielding the same counts within 5% was found relative to the rf phase for this case.

III. EXPERIMENTAL RESULTS

The experimental technique was to match the antenna input impedance for the 13.56 MHz rf power using a two-capacitor matching system at 3 mTorr of argon so that less than 5% of the incident power was reflected. The rf coupled power level and pulse width (4 ms) was set by the signal generator virtual interface: rf pulses were separated by a ten second period and were quite repeatable, with amplitude and phase variations from shot-to-shot at a given time and position under 5%. A typical ion saturation Langmuir probe curve for 2.3 kW net power coupled to the plasma measured at a radius of 5 cm at $z=25$ cm is shown in Fig. 3. Note that there is a density flattop from 1–2 ms after the rf power turns on which was obtained by tuning the matchbox network and it is during this period that the optical probe and wave B_z magnetic field data are collected. This constant density condition was created to reduce the complexity in analyzing data from the helicon source operation. The Langmuir probe-derived temperature corresponding to the Maxwellian background electron distribution is 3 eV for these plasmas. By moving the Langmuir probe along the z-direction at $r=5$ cm, we find that the density during the flattop peaks at $1.1\times10^{12}/\mathrm{cm}^3$ about 12 cm from the double-half-turn coil (located at $z=7.5$ cm). It then decreases to a lower density of $2\times10^{11}/\mathrm{cm}^3$ at $z=40$ cm and slowly decreases at further axial positions as shown in Fig. 4. The radial density profile is fairly flat in the interior region and drops off significantly for radii above 5 cm.

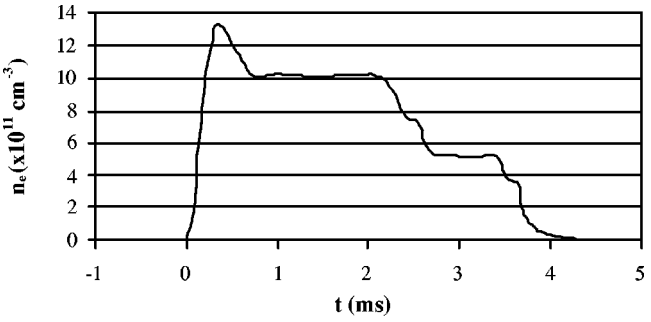

FIG. 3. Langmuir probe density trace versus time at $z=20$ cm, $r=3$ cm.

Wave B_z amplitude and phase measurements were carried out with a probe inserted at $r=4$ cm from the axis. Two magnetic loops separated by 2 cm that eliminate common mode electrostatic pickup were used to obtain the wave magnetic field values at different times during the shot. Figure 5 shows the axial variation of the B_z wave field amplitude and phase at $t=1.67$ ms. An earlier trace obtained at $t=1.01$ ms is also shown to show the slow time variation of the wave amplitude and phase during the density flattop. Note that near the antenna source at $z<10$ cm the wave phase has a standing wave character due to reflections from the conducting end plate at $z=0$ and propagates with increasing phase for $z>10$ cm away from the source. Local wave phase velocity is obtained from the B_z phase as $v_\phi = f(\Delta\phi/\Delta z)^{-1}\times 2\pi$. The wave B_z local phase velocity is minimum in the region near $z=15$ cm and then increases slowly along the axis until $z=40$ cm where it becomes very fast. Nearly resonant electrons with energies corresponding to this range of local phase velocities can readily excite the Ar II state from either the ground or ionized state.

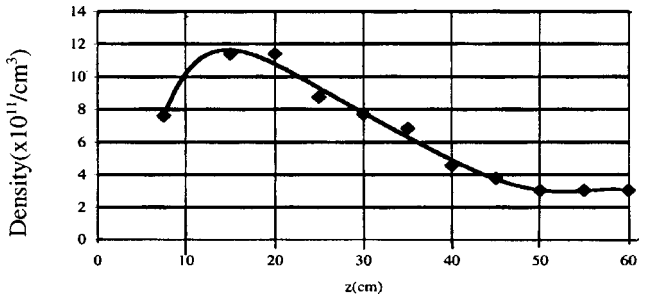

FIG. 4. Measured axial density profile at $r=3$ cm.

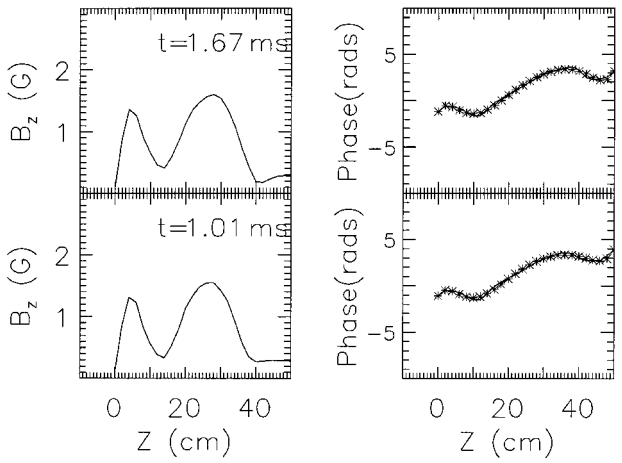

FIG. 5. Measured wave B_z amplitude and phase.

Figure 6 shows the variation of the peak in the 443 nm emission relative to a reference rf phase vs probe position for three runs of data taken for the above plasma density and wave phase velocity case. The optical spontaneous emission peak data correspond to three separate experimental runs. The bins 0–0.9 correspond to 36 degree or 10% increments of the 2π phase of the 13.56 MHz rf signal. A single emission peak is observed during a rf period, which indicates that it is caused by a traveling wave interaction. The wave accelerates some of the emission exciting electrons as it propagates axially away from the antenna. There is scatter in the peak phase since the 443 nm emission is due in part to an uncertainty in the emission lifetime of $\pm 10\%$ and a $\pm 7\%$ uncertainty for the photomultiplier transit time. Scatter can also arise due to the emission from a distribution of excitation electrons about the wave phase velocity as well. In addition, the local wave phase velocity is measured at $r = 4$ cm whereas the optical probe integrates the emission over the radius from $r = 0.75$ cm to 9 cm with a ± 5 degree beamwidth. The range of local electron resonant energies corresponding to the peak emission phase velocity corresponds to electron energies of 30–52 eV. This corresponds well to the local wave phase velocity over this range obtained from the B_z probe indicating that traveling wave–particle interactions play a significant role in fast electron creation for ionizing processes in the helicon source for this case.

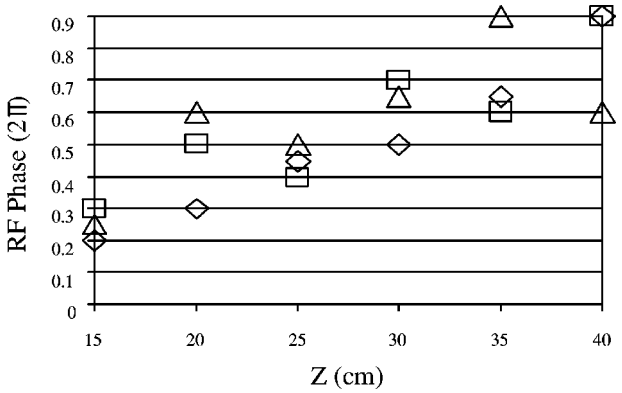

FIG. 6. Phase of the peak in modulated emission at 443 nm, measured by the optical probe for three separate runs represented by squares, diamonds, and triangles.

Figure 7 shows the modulation depth $I_{\mathrm{mod}}(\%) = ((I_{\max} - I_{\min})/I_{\max})$ of the 443 nm Ar II line during the 73.7 ns rf period collected by the optical probe as a function of the probe position. The modulation depth increases monotonically from 8% to 38% as one moves away from the antenna located at $z = 7.5$ cm. This indicates that an increasing fraction of the Ar II excitation occurs from wave-phase correlated excitations compared to the random background emission further from the antenna.

IV. HELICON WAVE, Ar II EMISSION AND WAVE IONIZATION ANALYSIS AND MODELING

A. Analysis of the wave magnetic field phase velocity and correlation with optical emission

We first analyze the measured wave magnetic field (B_z) local phase velocity and compare it to the observed velocity of the peak Ar II emission. The wave phase and amplitude for the 2.3 kW coupled power is shown in Fig. 5. An analysis of the local wave phase velocity and resonant electron energy, $E = m v_\phi^2/2$, was carried out for this case at $t = 1.67$ ms from the start of the pulse where the density is constant as shown in Fig. 8. The average B_z wave phase velocity for the traveling wave portion of the curve is 3.2×10^6 m/s corresponding to an average resonant electron energy of 29 eV over the range from $z = 12-30$ cm. The corresponding local differential resonant electron energies indicated by crosses over the same range are from 18–46 eV. The stars indicate the local wave phase and the smooth curve connecting the crosses serves as a guide to the eye for these data. It should also be noted that electrons interacting with the wave would have a distribution of velocities about the wave phase velocity. The electron resonant energies in this range are quite sufficient to excite the upper state for the 443 nm emission either from the ionic ground state or from the neutral state. The wave continues as a traveling wave until about $z = 35$ cm where it changes to a standing wave character. This can be due to the substantial axial density gradient in this region as well as a decrease by 10% in the static magnetic field over this range.

The 443 nm Ar II emission is modulated at the fundamental rf frequency which indicates a wave–electron interaction. The 443 nm optical emission peak moves with a resonant electron phase velocity, $v_{\phi 443} = \omega(\Delta\phi/\Delta z)^{-1}$, which is obtained from Fig. 6 in the range of $z = 10-40$ cm. The peak in the 443 nm emission travels at an average velocity range of $3.3-4.5 \times 10^6$ m/s for three separate runs in which 2.3 kW of wave power was coupled to the plasma. This range of energies corresponds to resonant electron energies of $E = 30-52$ eV. In order to cause modulated emission at the fundamental rf that persists (or even increases) downstream from the antenna, electrons from only one side of the distribution function must be accelerated by the wave to energies above the excitation threshold of the observed transition. This is sufficient energy to excite the upper Ar II state either by a two-step process or directly from the Ar neutral atom.

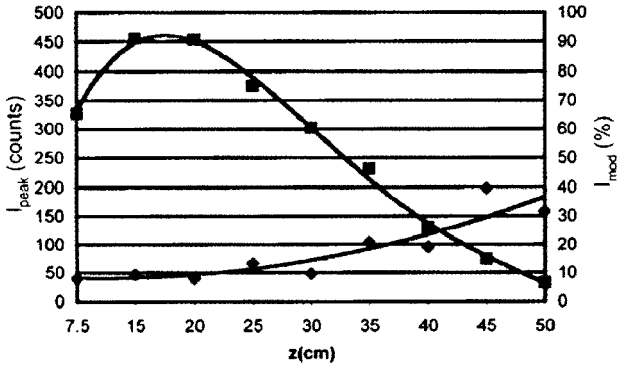

FIG. 7. Optical signal modulation index represented by diamonds as a function of axial position. The squares represent peak 443 nm emission counts.

It is interesting to note that the modulation of the emission at the rf period increases from 8–38% as one moves away from the antenna to $z=50$ cm. Significant contributions from fast electrons which travel at energies and velocities comparable to the helicon wave can directly excite the upper state of the 443 nm emission well away from the antenna.

B. ANTENAII modeling of the helicon mode

We used a model of the helicon wave coupling and wave propagation realized by the AntenaII[19] code. This is a linear wave code that allows a radial variation in plasma density and includes the full spectrum of the antenna and plasma conditions. It also incorporates collisional and Landau damping processes to compare with the experimental observations. The strong damping of the helicon wave observed experimentally can be modeled by an enhanced effective collision frequency. The code satisfies the experimental radial and axial conducting boundary conditions for the conducting end plate and the current jump condition corresponding to the double-half-turn coil. We model the antenna and plasma conditions to determine the axial wave magnetic field intensity and phase and compare it to that which is measured. The code also determines the self-consistent wave axial electric field, E_z, which is very difficult to measure but can be used in ionization modeling that incorporates nonlinear wave and trapped electron effects. Figure 9 illustrates the results for the case where the on-axis plasma density is set to $0.8\times10^{12}/\mathrm{cm}^3$ with a parabolic squared radial variation which models the axial average plasma properties over the 50 cm axial extent. A static magnetic field of 80 G and a 3 eV Maxwellian electron temperature with a total effective electron collision rate of $1\times10^7/\mathrm{s}$ is used to model the experimental conditions which is somewhat above the 3 eV Maxwellian electron collision frequency of $5\times10^6/\mathrm{s}$. This is done to model the enhanced damping of the helicon wave, which can be due to nonlinear processes. Note that the resulting modeled wave magnetic field shown in Fig. 9(a) is quite comparable to that measured by the B_z probe in Fig. 5. The peak wave magnetic field amplitudes are very close to those measured in the experiment and the axial wavelength of 25 cm is also quite comparable. The corresponding axial electric field, E_z, for a radius of 6.3 cm which simulates the average position in the radial sector that the axially centered optical probe samples for Ar II emission measurements is also shown in Fig. 9(b). This wave field is used in a model to carry out a calculation of the change in the electron distribu-

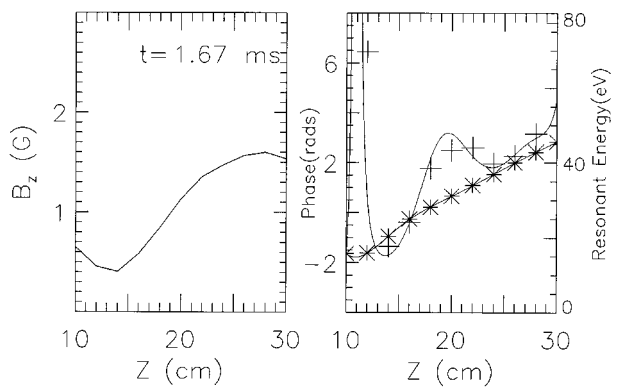

FIG. 8. Wave B_z magnitude and phase velocity resonant electron energy. The stars represent the measured wave phase and the crosses the corresponding local resonant electron energy.

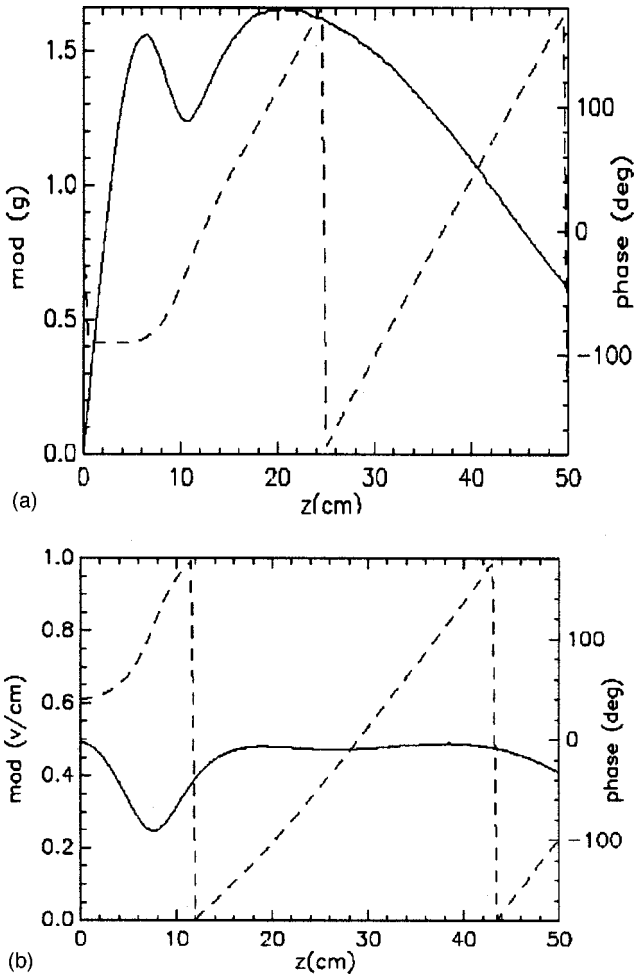

FIG. 9. AntenaII modeling of measured $B_z[\mathrm{mod}(g)]$ (a) at $r=4$ cm and corresponding wave E_z $[\mathrm{mod}(v/\mathrm{cm})]$ (b) at $r=6.3$ cm. The solid line represents amplitude and the dashed line represents phase.

tion function from a Maxwellian and the associated enhanced ionization for the experimental conditions.

C. Modeling of wave ionization of argon

We now consider a one-dimensional model of the helicon wave ionization of the argon gas. The model utilizes the measured B_z wave fields in the plasma that are well modeled by the AntenaII code[3,19] to predict the corresponding axial electric field, E_z, that accelerates electrons in a background 3 eV plasma. The code models the ionization rate of argon arising from an electron distribution function that is perturbed by an electrostatic wave component (E_z) of the helicon wave. Since an electron energy threshold of 15.6 eV is required to ionize argon, this model is sensitive to fast electron effects in the plasma and can illustrate enhanced ionization due to wave excited non-Maxwellian electrons when compared to a Maxwellian distribution. Previous theoretical work by Borg *et al.*[4] has carried out linear wave modeling for this process and demonstrated that under the appropriate conditions, substantial power flow from the antenna near zone wave fields results in a strong modification of the electron distribution which is evaluated to second order. Degeling[5,20] has generalized this result to include wave trapping and nonlinear wave–particle interactions and included a relaxational collision term which we use here. This model also evaluates the electron distribution function at different positions and times which is valuable in determining the non-Maxwellian character of the electrons in the presence of the wave.

The model operates by solving the collisionless equation of motion for individual electron trajectories, given by

$$m\frac{dv_z}{dt} = -eE_z(z,t),$$

as an initial value problem.[5,20] This is done by integrating backwards in time from the final velocities at a given position z_f and time t_f to obtain the initial velocities v_I at $z=0$, and the time t_i at which the electrons departed from $z=0$. The background electron distribution at $z=0$, $f_0(v_i)$, is taken to be a time independent Maxwellian with a 3 eV temperature. In the collisionless limit, these values of $f(v)$ only need to be mapped along the trajectories to give the distribution function at $z=z_f$. A finite collision frequency ν is modeled by considering that the probability of an electron being scattered onto a collisionless trajectory in the time interval dt and suffering no further collisions until it arrives at z_f after a time interval Δt is given by $\exp(-\nu\Delta t)\nu dt$. Electrons scattering onto the trajectories by collisions are considered in this model to have a Maxwellian distribution, so the distribution function at (z_f,t_f) is given by

$$f(v_f,z_f,t_f) = \int_{-\infty}^{t_f} f_0(v(t),z(t),t)\exp(-\nu(t_f-t))\nu dt.$$

Reif[21] has shown that this formulation is equivalent to the relaxation time approximation to the Boltzmann equation in which the collision term is given by $\nu(f_0-f)$. The same effective collision frequency of $\nu=10^7$ s^{-1} that was used by AntenaII to obtain the helicon wave field solutions is used in this model.

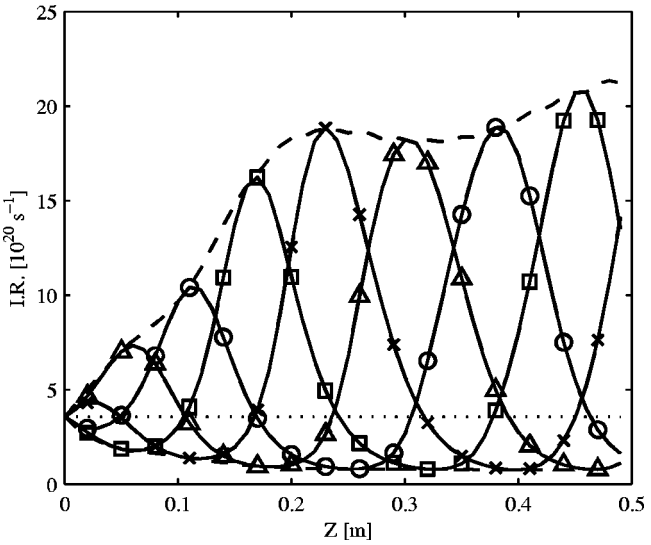

FIG. 10. Instantaneous ionization rate model for electric fields determined by the AntenaII code in Fig. 9(b). The instantaneous rate curves each correspond to a quarter rf period later in time. The dotted line corresponds to the ionization rate from a 3 eV Maxwellian distribution.

The ionization rate, I, is evaluated at a position and time and is given by

$$I = \int_0^\infty v_z f(v_z)\sigma(v_z)dv_z.$$

The argon ionization cross section $\sigma(v_z)$ and its coding used in our model for argon is taken from the work of Smith.[22]

Figure 10 illustrates the instantaneous ionization rate resulting from the modeled distribution function at four equally separated phases during a rf cycle, for our experimental conditions at $r=6.3$ cm. This radius corresponds to the average radial position the optical probe is sampling. The ionization rate resulting from a 3 eV Maxwellian distribution (which corresponds to the measured bulk electron temperature under similar conditions in WOMBAT) is indicated in the plot by a dashed line. The axial electric field component used for this calculation was obtained as a self-consistent field from a model of the experimental conditions from the AntenaII code as shown in Fig. 9(b). As mentioned earlier, these data were generated from a model of the plasma experimental conditions, for which good agreement was found between the modeled and measured wave B_z fields. Figure 10 shows that substantial enhancement of the ionization rate compared to a 3 eV Maxwellian occurs. The ionization rate is modulated, and is shown to propagate along the source at a velocity of 4×10^6 m/s, which corresponds to the wave phase velocity obtained from Fig. 9(a) for $z>10$ cm. A fast rise in the ionization rate envelope occurs which maximizes at $z=20$ cm, where the plasma density peaks, and is sustained downstream from the antenna position. This indicates a wave acceleration mechanism rather than local ionization occurring directly under the antenna. According to this

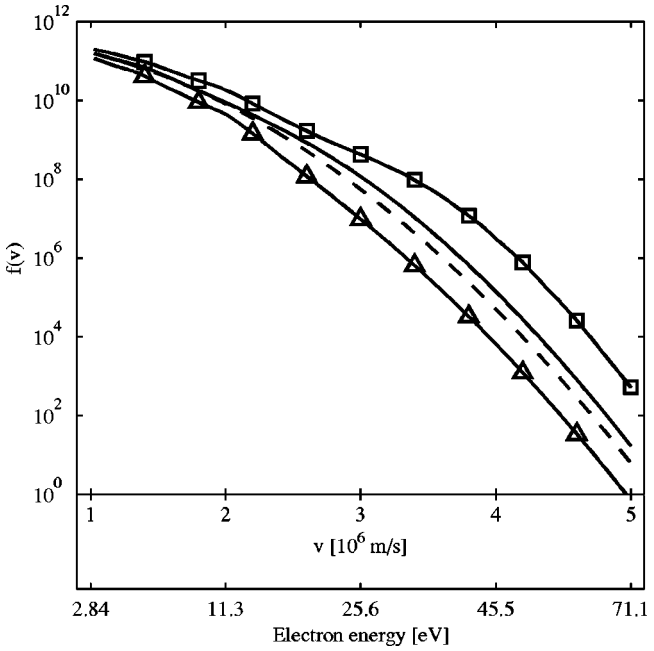

FIG. 11. Peak (squares), minimum (triangles), and time-averaged (solid line), wave-excited electron distribution function at $z=34$ cm. The dashed line corresponds to a 3 eV Maxwellian distribution.

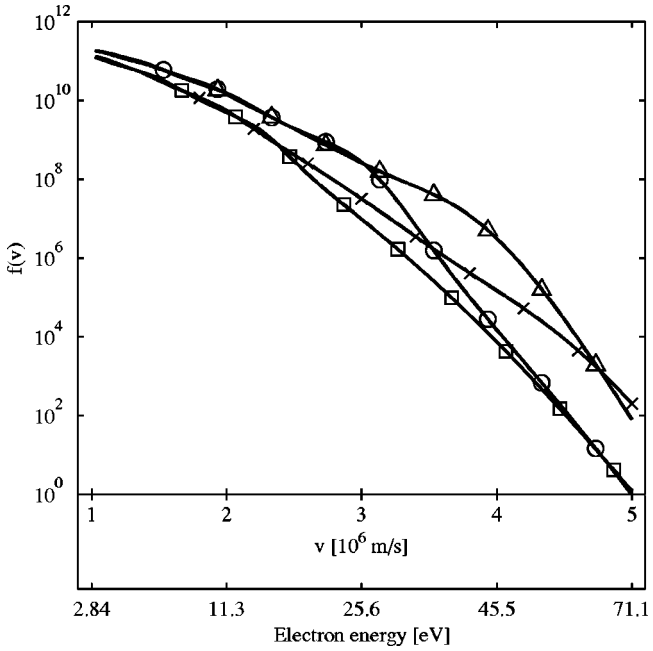

FIG. 12. Time dependence of wave-excited electron distribution function at $z=34$ cm. Each line connecting squares, crosses, triangles, or circles represents the distribution function a quarter of an rf cycle later which is 18.4 ns for the 13.56 MHz source.

model, this results in a substantial increase in the local time-averaged ionization above that of a Maxwellian for $z>15$ cm.

Figure 11 illustrates the envelope maximum and minimum, as well as the time-average electron distribution functions at $z=34$ cm. Figure 12 shows the instantaneous distribution function at the same position, at four equally separated phases during a rf cycle. These figures clearly show that the perturbation to the distribution function features an increase in the population of electrons with energies above the ionization energy of 15.6 eV that persists after time averaging.

This substantially modified distribution function at high energies will clearly affect the excitation rate of the Ar 443 nm emission in a similar fashion to the modeled ionization rate, either from direct or multi-step excitation processes. That is, the bursts in ionization found in this model that propagate downstream from the antenna at speeds comparable to the phase velocity will be accompanied by bursts in emission from the same distribution function. This supports the correlation between the propagation of the peak in the modulated Ar 443 nm emission and the local wave B_z phase velocity observed in the experiment.

V. SUMMARY

The mechanisms for helicon plasma source ionization and operation are quite sensitive to the density, magnetic field, pressure, antenna configuration and impedance matching. We have carried out wave magnetic field, optical and Langmuir probe measurements to examine fast and thermal electron contributions to plasma ionization on the WOMBAT facility. Spatio-temporal measurements of the 443 nm peak emission show that it is modulated at the source frequency. The peak density is observed to occur about 13 cm from the antenna, indicating that acceleration of the electrons from the antenna location in the direction of the helicon wave phase velocity occurs to maximize the argon ionization. For our plasma conditions, the peak Ar II emission phase propagates along the plasma at a speed comparable to the local helicon wave phase velocity. A significant variation between the local wave phase velocity and peak emission phase velocity is expected since there is an uncertainty due to the emission lifetime, photo-multiplier transit time and the distribution of excitation electrons about the wave phase velocity predicted by the ionization model.

The local phase velocity as measured by a magnetic radiofrequency probe corresponds to resonant electron energies of 18–46 eV in the region from 12–30 cm from the dual half-turn antenna. Wave resonant or accelerated electrons with these energies can readily excite the upper state of the Ar II 443 nm line from either the neutral or ionic ground state. The background emission level is due to the Maxwellian background contribution to the total emission, due to wave phase incoherent Maxwellian tail or multi-step excitation processes.

Computer simulations of the wave–plasma interaction for the axial component of the wave electric field corresponding to the measured wave axial magnetic field phase were carried out. They show that enhanced ionization and modulation at the wave frequency compared to a 3 eV Maxwellian occurs due to the wave field interaction with the electrons with a local maximum ionization rate close to where the measured density peaks at 13 cm downstream from the antenna. An increase in the distribution function for electrons in the energy range (20–45 eV) comparable to the wave phase resonant velocities and energies corresponding

to the peak Ar II emission speed is predicted. This implies that a substantial contribution to ionization due to non-Maxwellian electrons under these helicon source conditions exists.

ACKNOWLEDGMENTS

This research was supported by National Science Foundation (NSF) Grant No. ECS-9905948 and AFOSR Grant No. F49620-00-1-0191. J.S. also thanks the Australian National University for their generous support while there.

[1]R. Boswell and F. Chen, IEEE Trans. Plasma Sci. **25**, 1229 (1997).
[2]F. Chen and R. W. Boswell, IEEE Trans. Plasma Sci. **25**, 1245 (1897).
[3]Y. Mouzouris and J. Scharer, Phys. Plasmas **5**, 4253 (1998).
[4]G. G. Borg, J. Bright, and I. V. Kamenski, Plasma Phys. Controlled Fusion **48**, 987 (1998).
[5]A. Degeling and R. Boswell, Phys. Plasmas **4**, 2748 (1997).
[6]S. Cho and J. G. Kwak, Phys. Plasmas **4**, 4167 (1997).
[7]A. Degeling, N. Mikhelson, R. W. Boswell, and N. Sadeghi, Phys. Plasmas **5**, 572 (1998).
[8]R. Chen and N. Herskowitz, Phys. Rev. Lett. **80**, 4677 (1998).
[9]A. Ellingboe, R. Boswell, J. Booth, and N. Sadeghi, Phys. Plasmas **2**, 1807 (1995).
[10]A. Molvik, T. D. Rognlien, J. A. Byers, R. H. Cohen, A. R. Ellingboe, E. B. Hooper, H. S. McLean, B. W. Stallard, and P. A. Vitello, J. Vac. Sci. Technol. A **14**, 984 (1996).
[11]X. Guo, J. E. Scharer, Y. Mouzouris, and L. Louis, Phys. Plasmas **6**, 3400 (1999).
[12]P. Zhu and R. Boswell, Phys. Fluids B **3**, 869 (1991).
[13]A. J. Perry, D. Vender, and R. W. Boswell, J. Vac. Sci. Technol. B **9**, 310 (1991).
[14]G. Giroult-Matlakowski, C. Charles, A. Durandet, R. W. Boswell, S. Armand, H. M. Persing, A. J. Perry, P. D. Lloyd, S. R. Hyde, and D. Bogsanyi, J. Vac. Sci. Technol. A **12**, 2754 (1994).
[15]P. A. Keiter, E. E. Scime, and M. M. Balkey, Phys. Plasmas **4**, 2741 (1997).
[16]F. R. Chang Diaz, J. P. Squire, R. D. Bengston, B. N. Breizmann, F. W. Baity, and M. D. Carter, *Proceedings of the 36th AIAA/ASME/ASEE Joint Propulsion Conference* (American Institute of Aeronautics and Astronautics, Reston, VA, 2000), No. 2000-3756.
[17]D. D. Blackwell and F. Chen, Plasma Sources Sci. Technol. **10**, 226 (2001).
[18]V. Vujnovic and W. L. Wiese, J. Phys. Chem. Ref. Data **21**, 919 (1992).
[19]Y. Mouzouris and J. Scharer, IEEE Trans. Plasma Sci. **24**, 152 (1996).
[20]A. Degeling, ''Plasma production in a large volume helicon wave discharge,'' Ph.D. thesis, Australian National University, Canberra, 1999.
[21]F. Reif, *Fundamental of Statistical and Thermal Physics* (MacGraw-Hill, New York, 1965).
[22]H. Smith, ''Computational studies of an asymmetric rf plasma discharge using particle in cell techniques,'' Ph.D. thesis, Australian National University, Canberra, 1996.